Study of some characteristics describing the oxidation of a {m, m'}-based {30Cr, 1C, 15Ta} containing alloy during heating up to high temperature and the oxide scales behavior during post-{isothermal stage} cooling. part 1: {m, m'}={Ni, Co}

Gaël Pierson[1,2], Kevin Duretz[1,2], Thierry Schweitzer[2], Elodie Conrath[3], Patrice Berthod[1,2,3]*

[1]University of Lorraine, (FRANCE)
[2]Faculty of Sciences and Technologies, (FRANCE)
[3]Institut Jean Lamour (UMR 7198), Team 206 "Surface and Interface, Chemical Reactivity of Materials"
B.P. 70239, 54506 Vandoeuvre-lès-Nancy, (FRANCE)
E-mail : Patrice.Berthod@univ-lorraine.fr

ABSTRACT

An alloy based on nickel and cobalt in equal parts, rich in chromium and containing a dense TaC network in its microstructure was tested in oxidation at high temperature in dry synthetic air. The thermogravimetry tests were performed at 1000, 1100 and 1200°C during 40 hours. The mass gain files were plotted versus temperature and exploited to specify the oxidation start during heating and spallation start during cooling temperatures as well as the successive parts of mass gain achieved during heating and during the isothermal stage. The three mass gain kinetics were globally parabolic and the oxidation rates were characteristic of a chromia-forming behaviour. The oxidation start temperature at heating was seemingly the same for the three tests. The higher the temperature the higher the heating mass gains and the isothermal mass gain, and also the higher the temperature of spallation start at cooling. The mass gain obtained at the end of heating represents about 5% of the total mass gain.   © 2015 Trade Science Inc. - INDIA

INTRODUCTION

Most of carbides-strengthened superalloys contain are based either on nickel or cobalt, or on both of them together. Nickel is generally present in cobalt-based alloys to extend the FCC matrix temperature range of stability while the presence, in nickel-based alloys, of cobalt as an alloying element brings additional mechanical resistance. Thus, generally, one of the two elements plays the role of the base one while the other one is considered as an alloying element.

A third element is also often present in such alloys devoted to high temperature applications: chromium. This later one brings hot chemical resistance against both oxidation and corrosion to alloys involved as structural materials in the aero-engines and hot industrial processes[1-4] at elevated temperature, corrosion-resistance also exploited at much lower temperatures in other fields

as for prosthetic dentistry[5-7]. In the first case, especially concerned by this work, carbon is present too in the alloys to form carbides, in some case precisely with chromium to achieve high hardening of the alloys for reach high creep resistance[8]. This hardening is more intense when the carbon contents are higher; but because of the still continuity of the metallic matrix a minimum of ductility is preserved and the combination of that with high hardness leads to interesting wear resistances[9-13].

Nickel-based alloys containing a few wt.% of Co and Cobalt-based alloys with 5 to 10 wt.% of Ni in their chemical composition are rather numerous. Among them the ones which are reinforced by chromium carbides are not rare. In contrast chromium-rich alloys containing almost the same quantities in nickel and in cobalt are much less numerous and seemingly no of them contain the very stable tantalum carbides instead chromium carbides. This is the reason why a study was initiated about chromium-rich alloys based on Ni and Co simultaneously, and containing high levels in carbon and tantalum to promote the development of a dense network of tantalum carbides. The first results concerning the preliminary thermodynamic calculations and the obtained as-cast microstructures were presented in an earlier article[14]. The purpose of the present work is to specify some characteristics of the oxidation behaviour of the same alloys at high temperature.

EXPERIMENTAL

The material the high temperature oxidation of which is here studied is an alloy wished with 30wt.%Cr, 1wt.%C, 15wt.%Ta and equal contents in nickel and cobalt, 27wt.% each. One can remind[14] that the obtained chemical composition globally well fitted the targeted one, with 26.04±1.15wt.%Ni, 25.90±1.01wt.%Co, 29.68±1.17wt.%Cr, and 18.37±3.32wt.%Ta (the carbon content being not controllable by Energy Dispersive Spectrometry). In the microstructure observed after elaboration, illustrated in Figure 1 by a micrograph taken with a Scanning Electron Microscope (SEM) in Back Scattered Electrons (BSE) mode, the carbides network is essentially composed of TaC (in white in the SEM/BSE micrographs) which are of two natures: blocky pre-eutectic ones

and script-like eutectic ones. Their surface fraction, as measured by image analysis, is very high (12.47±4.04 surf.%) while the chromium carbides, which are also present, are much more rare (0.36±0.29 surf.%). This dense carbide network leads to rather high hardness for the alloy in its as-cast condition (slightly higher than 300 Hv_{30kg}).

During the cutting carried out to obtain the part for the metallographic examinations, other parts were also machined, to obtain three parallelepipeds of about 3mm × 7mm × 7 mm, which were ground with SiC papers of grade 1200. The edges and corners were smoothed. The oxidation tests were realized in dry synthetic air (80% N_2-20% O_2) using a SETARAM TGA92 92-16.18 thermobalance. The heating was realized at +20K min^{-1}, the isothermal stage at 1000, 1100 or 1200°C during 40 hours, and the cooling rate at -5K min^{-1}.

The mass variations were recorded every 32 (test at 1000°C) or 33 (1100&1200°C) seconds. The mass gain files were corrected from the air buoyancy variations and plotted as mass gain versus temperature and exploited to specify the following characteristics:

Heating

- temperature at which the mass gain is significant
  enough to be detected by the micro-balance,
- eventual determination of the activation energy (if linear part in the curve describing the instantaneous linear mass gain rate variation with temperature, plotted according to the Arrhenius scheme),
- total mass gain achieved during the whole heating between the start of oxidation and the beginning of the isothermal stage),
- final linear mass gain rate when temperature reaches the isothermal stage one;

Isothermal stage

- global shape of the mass gain curve when plotted versus time (parabolic or not, jumps or not),
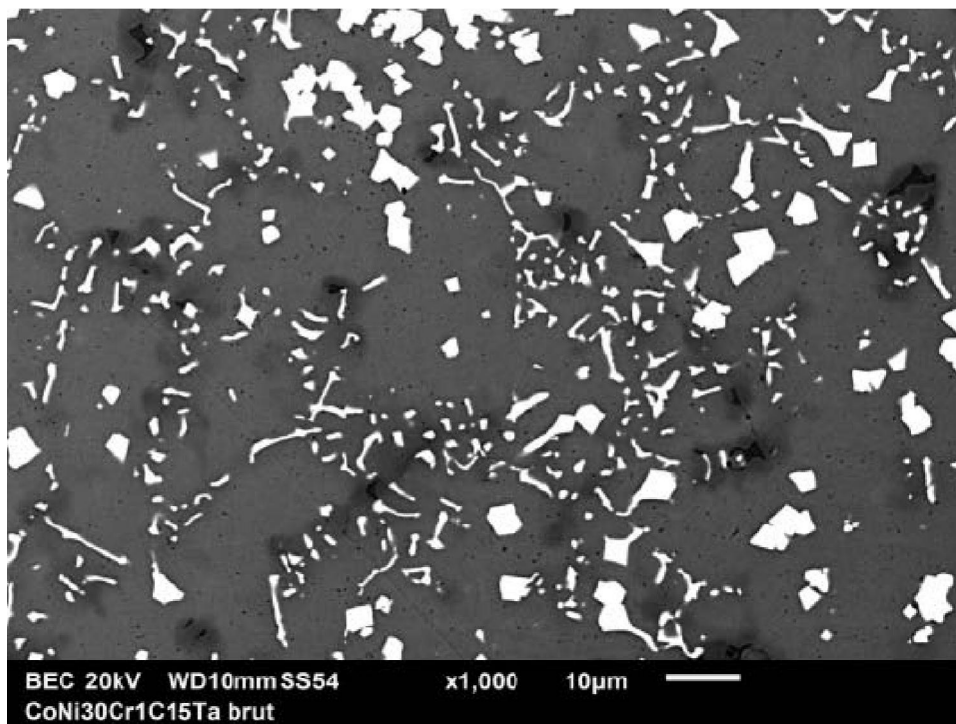- total mass gain exclusively achieved during the isothermal stage;

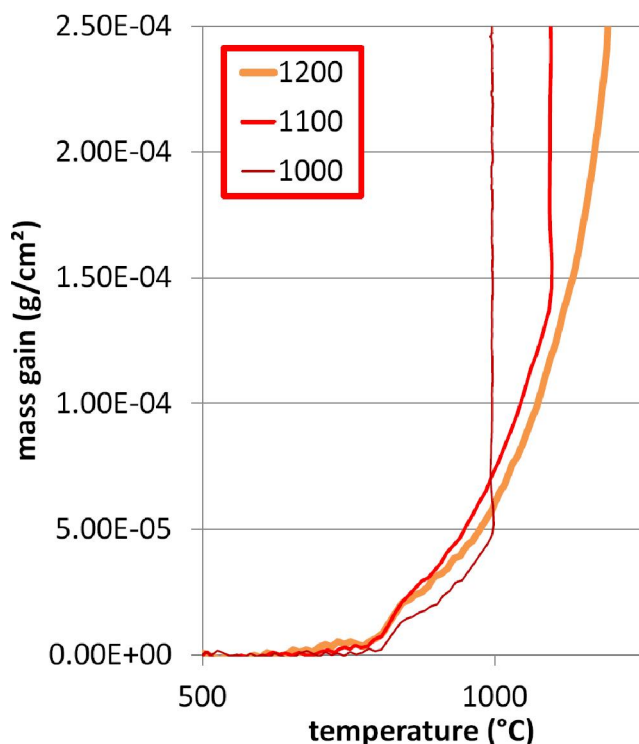**Figure 1 : SEM/BSE micrograph illustrating the as-cast microstructure of the studied alloy**

Figure 2 : Enlarged view of the mass gain curves recorded during heating until reaching 1000, 1100 or 1200°C

Cooling

- Temperature at which the mass variation accelerates or becomes irregular (start of scale spallation),

TABLE 1 : Values of the temperatures at which the mass gain by oxidation during heating has become significantly high enough

1000°C-test	1100°C-test	1200°C-test	reproducibility
795.8	783.0	797.2	rather good

- final mass variation.

RESULTS AND DISCUSSION

Oxidation during heating

The heating parts of the mass gain curves plotted versus temperature are presented together in Figure 2. It appears first that the common parts of the 1000°C-curve, the 1100°C-curve and the 1200°C curve (up to 1000°C) are almost superposed; the same comment can be made for the common parts of the 1100°C-curve and the 1200°C-one (between 1000 and 1100°C) since they are "parallel" (greater shift inherited from the small first one over the [1000, 1100°C] range). However, despite this rather good correspondence between the three curves obtained for the same alloys on the same temperature range (by parts) the temperatures of oxidation start (defined as being the ones at which the mass gain is high enough to be detected by the thermo-balance)
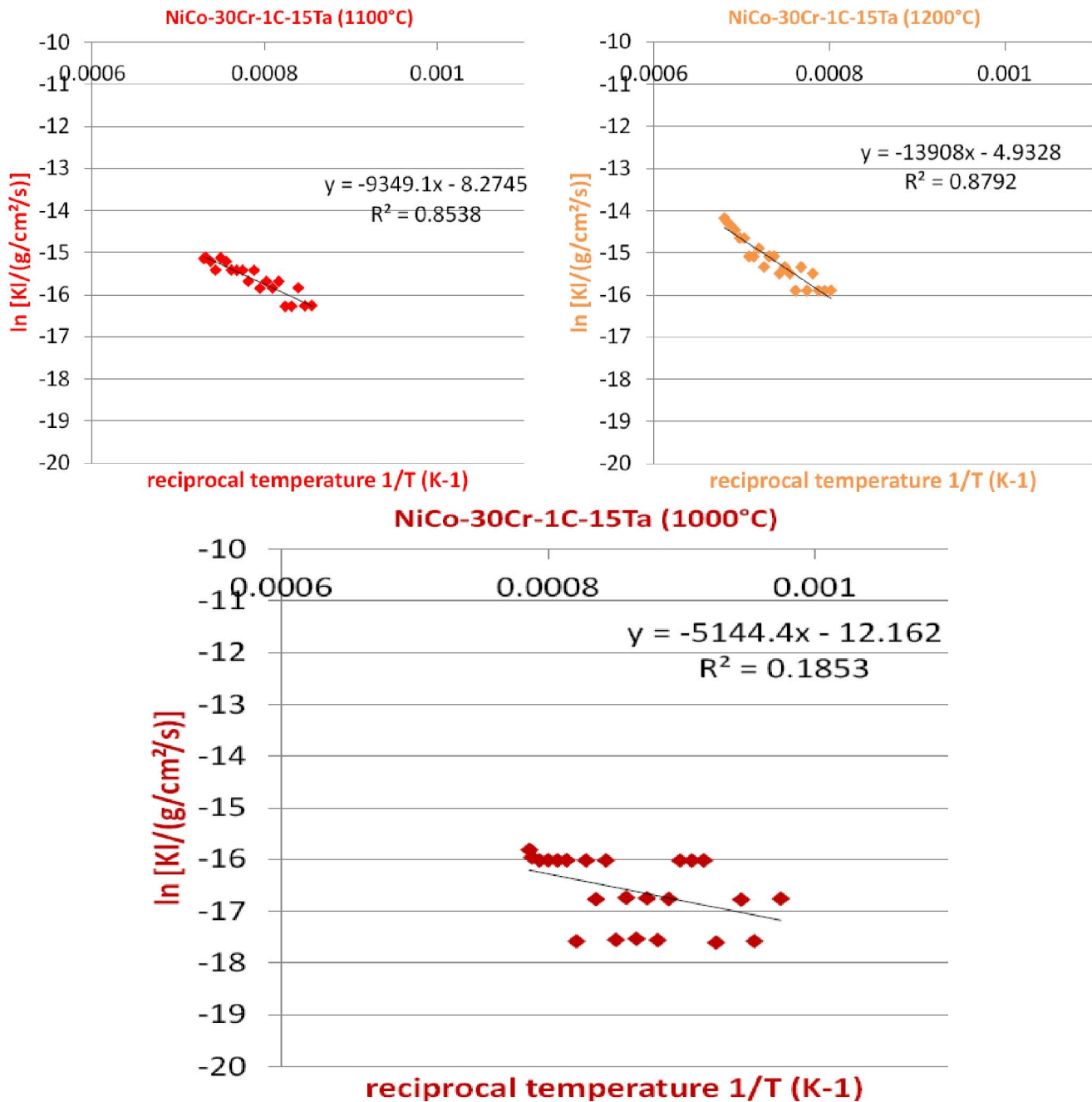
Full Paper

Figure 3 : Arrhenius plot of the instantaneous linear oxidation constant over the whole heating (or only a part if the point's cloud is not straight elongated); values of the slope of the regression straight line for deducing the values of activation energies (displayed in TABLE 2)

are almost the same (TABLE 1). Indeed there are spread over only less than 15°C.

Over these temperatures of oxidation start the instantaneous linear kinetic constant increases more and more rapidly when temperature increases during the heating, this letting thinking to an exponential increase with temperature. The Arrhenius plot confirms this over the whole heating from oxidation start

or only on the high temperature part of the heating, since the points' clouds are globally elongated along a straight line. The slope of the regression straight line led to the values of activation energies listed in the first line of TABLE 2. These values are of the usual order of magnitude (several tens of kJ/Mol) but they are obviously not the same for each test, this evidencing a lack of reproducibility which may

Full Paper

TABLE 2 : Values of the activation energies characterizing the dependence on temperature of the linear oxidation constant K_l issued from the successive values of K_l noted during the heating (over the linear part of the Arrhenius plot); value of the K_l value at the start of the isothermal stage

Q (J/Mol) issued from the ln ((dΔm/S)/dt) plot versus 1/T (K) during heating	1000°C-test	1100°C-test	1200°C-test
	42770	77728	115631
Final value of K_l (end of cooling, beginning of the isothermal stage ($\times 10^{-8}$g/cm²/s)	8.83	29.86	77.32
Mass gain at the end of heating (mg/cm²)	0.052	0.146	0.264

TABLE 3 : Values of the temperatures at which the mass gain by oxidation during heating has become significantly high enough to be detected by the thermobalance

Oxidation test	Mass gain at the end of heating (mg/cm²); Proportion / heat.+isoth. (%)	Mass gain at the end of the isoth. stage (mg/cm²) (sum of ← and →)	Isothermal mass gain (mg/cm²); Proportion / heat.+isoth. (%)
1200°C-test	0.264 (5.16%)	5.116	4.852 (94.84%)
1100°C-test	0.146 (4.26%)	3.435	3.289 (95.74%)
1000°C-test	0.052 (3.94%)	1.313	1.261 (96.06%)

result from different oxidation sequences (preferential oxidation of Co and/or Ni, or of Cr or of Ta) during the heating.

The second line of TABLE 2 contains the values of the final value of (dΔm/S)/dt when temperature reaches the stage one. This ultimate value of K_l effectively increases with temperature, showing that oxidation is, at the beginning of the isothermal stage, logically faster when the stabilized temperature is higher.

The mass gains achieved during the whole heating are displayed in the third line of TABLE 2. The value is logically higher for a higher temperature.

Isothermal oxidation

When plotted as mass gain versus time the isothermal oxidation curves are globally parabolic. There are some irregularities during the first ten hours (small jumps) but they become more parabolic thereafter. When plotted versus temperature (after having corrected the mass gain files from the air buoyancy variations) the three curves present a first part which quit the abscissa axis leading to the final mass gain already given in the last line of TABLE 2. Thereafter, in this type of representation the oxidation curve becomes a vertical straight line the length of which represents the part of mass gain which is isothermally realized. The values of this isothermal mass gain are given in TABLE 3 (last col-

umn). To obtain them the value of the mass gain at the end of the isothermal stage was red in the file and subtracted by the value of the total mass gain achieved during the heating (already given in TABLE 2 but reminded in TABLE 3). Logically the higher the temperature the higher the mass gain achieved during the 40 hours of isothermal oxidation. The calculation of the proportions in TABLE 3 shows that this isothermal mass gain is of course the major part of the total mass gain (95-96%) but it is also true that the mass gain already realized when the isothermal stage starts is significant (4-5% of the final mass gain before cooling).

Phenomena at cooling

The third part corresponds to the cooling during which oxidation may continue but slower and slower. After an eventual jump in mass gain (probably bending of the external scale - due to thermal contraction of the alloy faster than the scale's one - followed by a rapid re-oxidation of the denuded alloy), the mass decreases rapidly and irregularly: this is the spallation of the external oxide scale which starts at a given temperature and which leads to final mass which may be lower than the previous one if spallation was particularly severe. Sometimes final mass variations may be negative although that the main part of the experiment was character-

TABLE 4 : Values of the temperatures at which spallation started during the cooling and final mass variation after return at room temperature

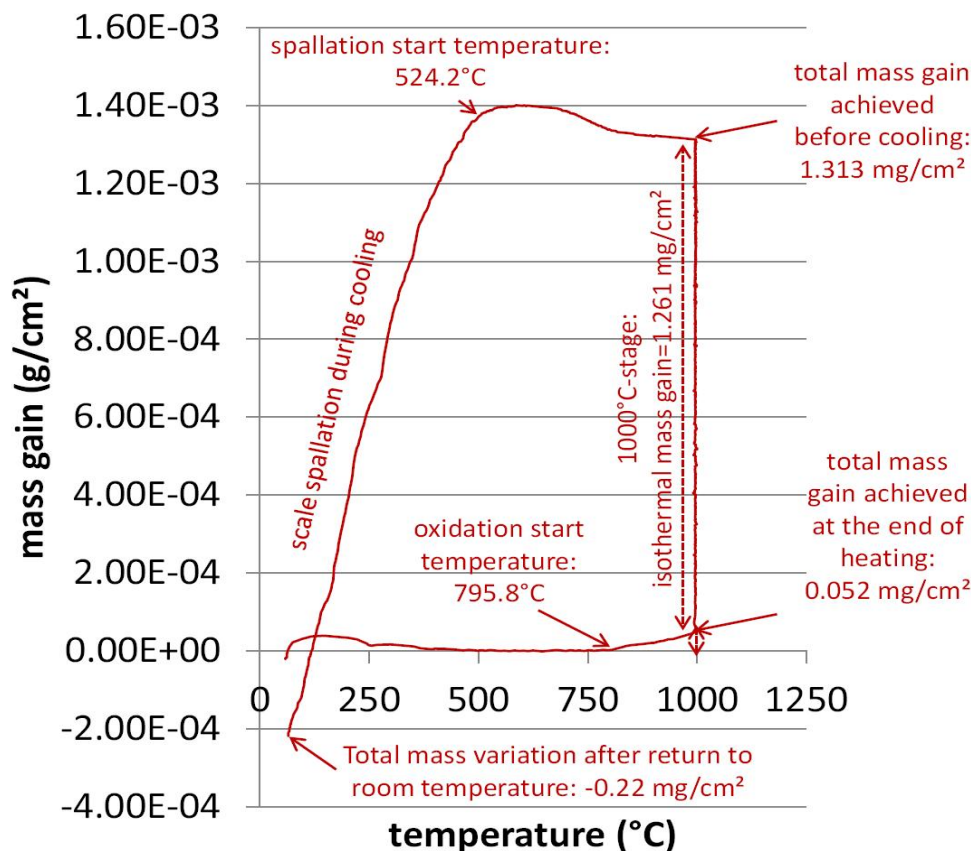| Oxidation test	Temperature of start of the cooling-induced scale spallation (°C)	Final mass variation at the end of the whole thermal cycle (mg/cm²)
1200°C-test	956.2	-5.33
1100°C-test	880.2	-2.16
1000°C-test	524.2	-0.22

Figure 4 : The {mass gain versus temperature}-plot for the whole thermal cycle of the 1000°C-oxidation test

ized by a mass gain all time (except the second part of cooling of course): the mass of oxygen remaining over the oxidized sample combined with the metallic elements may be lower than the mass of metallic elements lost as oxides when the scale – partly or wholly - quitted the samples.

The values of the temperatures at which oxide spallation started during the cooling for the three experiments as well as the final mass variations are given in TABLE 4. It appears that the highest the stage temperature the higher the spallation start temperature, and second the highest the stage temperature the lower the algebraic final mass variation.

Graphical summary

The whole curves plotted as mass gain versus

temperature are presented in Figure 4 for the 1000°C-test, Figure 5 for the 1100°C-test and in Figure 6 for the 1200°C test, with in each case the designation by arrows of the locations where the values of temperatures or of mass variations were red, as well as the obtained values already presented in the successive tables.

General commentaries

Plotting the mass gain files as mass gain versus temperature, after having had a rapid look to the more classical representation versus time to see the global shape of the curves, allows a complete characterization of the whole oxidation test.

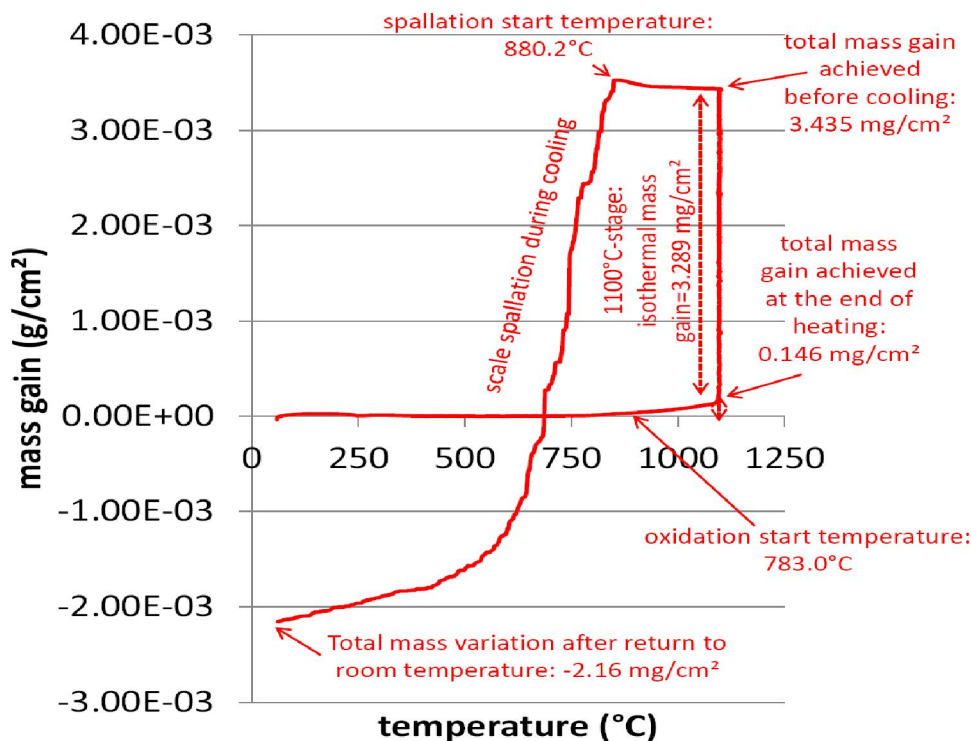The kinetic of oxidation of this alloy was thus

Full Paper

Figure 5 : The {mass gain versus temperature}-plot for the whole thermal cycle of the 1100°C-oxidation test
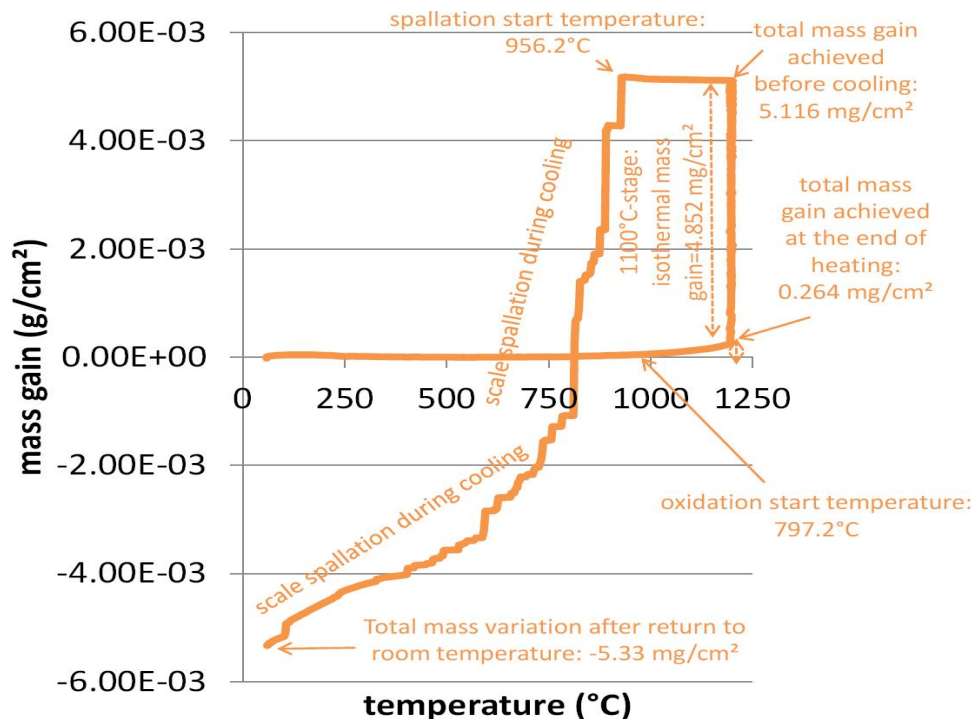

Figure 6 : The {mass gain versus temperature}-plot for the whole thermal cycle of the 1200°C-oxidation test

globally parabolic, with a shape only a little perturbed by small irregularities/jumps in the first ten hours.

For the given thermo-balance the oxidation started in the three cases at almost the same temperature of about 790°C but it is true that this result depends on the accuracy of this thermo-balance. The result should be slightly different if the tests were carried out with other apparatus; probably: the lower the thermo-balance accuracy the higher the oxida-

tion start temperature. In reality oxidation started at much lower temperature but the method used here should give interesting indications between the differences of behaviour of different alloys tested with the same thermo-balance for the same atmosphere and heating rate.

After having observed that the total mass gain achieved during heating and the isothermal mass gain both increase with the stage temperature, it was also interesting to see that the first one is significant (4-5%) although it represents only a little part of the total mass gain achieved before cooling. However it is also true that its proportion depends on the stage duration: here 40 hours was rather short. For longer isothermal stages the part of heating in the mass gain should be lower.

The isothermal mass gains were comparable to what may be obtained with chromia-forming alloys for the same temperature and durations, and it is probable that the alloy showed the same behaviour.

The cooling induced severe spallation of the formed oxide scale, as demonstrated by the cooling parts of the curve which finish with negative mass variations. These ones are similar, or at least of the same order of magnitude as the total mass gain before cooling. Taking into account that the mass gain involved only the oxygen arrival on the samples while the mass loss was a loss of both metals and oxygen combined in oxides, probably only a part of the oxide scale has quitted the samples by spallation during the cooling. Thus some external oxides remained on the oxidized samples which will allow characterizing them by post-mortem metallographic observations to better know what are the oxides which formed.

Always concerning spallation it seems that the mass of oxides initially formed tend, not only to induce more negative mass variations after return to room temperature, but also to accelerate the spallation itself in term of start temperature. But it is true that this is may be more the decrease in temperature before spallation rather than the temperature of cooling start itself which must be taken into account.

CONCLUSIONS

These oxidation tests, and the method followed to treat the mass gain files gave numerous indica-

tions about the behaviour of this alloy based on nickel and cobalt at equal contents, rich in chromium and reinforced by numerous TaC carbides. Among them there are data about the isothermal mass gains and about the spallation at cooling which will be verified by post-mortem characterization of the oxidized samples: observation of the surfaces concerning the lost parts of oxide scale and the natures and external structure of these oxides, and cross-section observations of the remaining parts of the scales through their total thickness as well as the state of the sub-surface of the samples. This will be the subject of a future extension of this work[15].

REFERENCES

[1] M.A.Engelman, C.Blechner; The New York Journal of Dentistry, **46**, 232 **(1976)**.

[2] E.F.Huget, N.Dvivedi, H.E.Cosner; The Journal of the American Dental Association, **94**, 87 **(1977)**.

[3] P.Berthod, J.L.Bernard, C.Liébaut; Patent WO99/16919.

[4] P.Kofstad; 'High Temperature Corrosion', Elsevier applied science, London **(1988)**.

[5] C.T.Sims, W.C.Hagel; "The superalloys", John Wiley & Sons, New York **(1972)**.

[6] M.J.Donachie, S.J.Donachie; 'Superalloys: A Technical Guide" (2nd Edition), ASM International, Materials Park **(2002)**.

[7] D.A.Bridgeport, W.A.Brandtley, P.F.Herman; Journal of Prosthodontics, **2**, 144 **(1993)**.

[8] E.F.Bradley; 'Superalloys: A Technical Guide', ASM International, Metals Park **(1988)**.

[9] A.Klimpel, L.A.Dobrzanski, A.Lisiecki, D.Janicki; Journal of Materials Processing Technology, **164-165**, 1068 **(2005)**.

[10] Z.T.Wang, H.H.Chen; Mocaxue Xuebao Tribology, **25**, 203 **(2005)**.

[11] H.Han, S.Baba, H.Kitagawa, S.A.Suilik, K.Hasezaki, T.Kato, K.Arakawa, Y.Noda; Vacuum, **78**, 27 **(2005)**.

[12] D.Zhang, X.Zhang; Surface and Coating Technology, **190**, 212 **(2005)**.

[13] B.Roebuck, E.A.Almond; Int.Mater.Rev., **33**, 90 **(1988)**.

[14] K.Duretz, G.Pierson, P.Berthod; Materials Science: An Indian Journal, in press.

[15] G.Pierson, K.Duretz, P.Villeger, P.Berthod, E.Conrath; Materials Science: An Indian Journal, to be submitted.